https://doi.org/10.48048/tis.2022.1588

Numerical Study of Non-Newtonian Fluid in a Cavity with Corrugated Bottom Wall Using Buongiorno's Mathematical Model

Hure Zannatul Mawa[1], Md. Abul Kalam Azad[2], Chowdhury Sadid Alam[3] and Md. Mustafizur Rahman[4,*]

[1]Department of Civil Engineering, Presidency University, Gulshan 1212, Bangladesh
[2]Department of Natural Sciences, Islamic University of Technology, Gazipur 1704, Bangladesh
[3]Department of Mechanical and Production Engineering, Islamic University of Technology, Gazipur 1704, Bangladesh
[4]Department of Mathematics, Bangladesh University of Engineering and Technology, Dhaka 1000, Bangladesh

([*]Corresponding author's e-mail: m71ramath@gmail.com, mmustafizurrahman@math.buet.ac.bd)

Received: 28 December 2021, Revised: 4 February 2022, Accepted: 28 February 2022, Published: 10 November 2022

Abstract

A 2-dimensional computational analysis is carried out for a time dependent double diffusive mixed convection flow using non-Newtonian nanofluid. A square-shaped cavity with a corrugated bottom wall is taken with higher temperature and concentration on the top wall. The physical model under consideration is represented by a set of governing equations and solved using the Galerkin weighted residual method based on Finite Element Analysis. Solutions are done for 4 controlling parameters such as Richardson number (Ri = 0.1 - 15), Lewis number (Le = 0.5 - 3), and thermophoresis parameter (Nt = 0.2 - 0.9), and Brownian motion parameter (Nb = 0.2 - 1.0) at different values of τ. For the aforementioned parameters, heat and mass transfer rates, temperature distributions, velocity distributions, and mass distributions in terms of isotherm, streamlines, and iso-concentration are graphically presented. It has been observed that for higher values of Ri, both Nu_{av} and Sh_{av} increased while Le decreased for higher values of Nt at any fixed time. It is worth noting that the considered parameter exhibits consistent behavior after a while.

Keywords: Non-newtonian nanofluid, Buongiorno's mathematical model, Mixed convection, Corrugated bottom wall, Power-law fluid

Introduction

Non-Newtonian nanofluids are extensively used in many industries and technological aspects like as polymer melts, biological analysis, mixture of aggregates, pigmented liquids, and glues etc. Nanofluids can dramatically increase heat transfer levels in a variety of applications, such as nuclear reactors, industrial cooling, transportation, nanoelectromechanical systems, heat pumps, fiber and fine-grained insulation, chemical catalytic reactors, petroleum storage tanks, lined beds, and radioactive waste repositories [1-3]. Nazari *et al.* [4] numerically investigated the mixed convection flow of a non-Newtonian Al2O3-water nanofluid in a square cavity with hot and cold lids. They found that increasing nanoparticle volume fraction and decreasing Darcy number improve temperature distribution and decrease dimensionless temperature. Pawar *et al.* [5] performed an experimental analysis for both the fluids - Newtonian and non-Newtonian; on non-isothermal instable state conditions and isothermal steady-state in helical coils. The research found Newtonian fluids such as water and glycerol - water mixture and non-Newtonian fluids such as dilute sodium carboxymethyl cellulose (SCMC), aqueous polymer solutions and sodium alginate (SA). Zhixiong *et al.* [6] mathematically tested the non-Newtonian nanofluid flow of mixed convection in a H-shaped cavity using the Boussinesq approximation. They considered rotating cylinders inside the cavity. They revealed that the direction in which the cylinder rotates influences the strength of the flow field. Yoshino *et al*. [7] developed a Boltzmann lattice (LBM) based unique computational approach for non-Newtonian incompressible fluid flow. Estimates imply that the approach is useful for functional non-Newtonian fluid flows, for example, shear-thickening (dilatant) flows and shear-thinning (pseudoplastic) flows.

Heat transfer and fluid flow of corrugated channels have received significant study interest in recent years due to the widespread use of thermal appliances like heat exchangers. Because of the secondary flow regimes that form along the corrugated walls, fluid mixing and heat transfer efficiency will improve as fluid flows through these channels. Work on new passive techniques appears to be quite significant due to the

growing desire for a more compact design of heating systems and improved efficiency by various engineering applications. Nanoparticles added up with the base fluid for this reason will enhance the thermal conductivity of base fluid[8]. Goodarzi *et al.* [9] used the lattice Boltzmann method on a nanoscale to develop and predict fluid flow and air heat transfer in a 2-dimensional inclined lid driven cavity with a large heat source inside the cavity. They looked at pure natural convection and mixed convection for LBM and discovered that the considered model is suitable for simulating the system and that inclined angle is important for higher Richerson numbers. Rahman *et al.* [10] studied the impacts of performance characteristics on double-diffusive flow with the corrugated bottom wall in a triangular cavity. It has been found that flow intensity of Rayleigh numbers can be regulated by wavelength. Alireza *et al.* [11] used numerical simulations to optimize the attack angle range of 450 to 1,350 for a water/Ag nanofluid in an elliptical cavity. They discovered that increasing the attack angle decreases surface stress and fluid adhesion to the hot surface, owing to gravity's weakening of the tangential velocity component. Alireza *et al.* [12] then looked at the impact of horizontal and vertical elliptic blocks inside a square cavity filled with MWCTs-water nanofluid. They discovered that the horizontal block exhibits the highest mean heat transfer rate at $Ri = 0.01$. Buren *et al.* [13] studied the electromagneto-hydrodynamic flow (EMHD) within a micro parallel channel where walls are corrugated. They show the corrugations can increase the mean EMHD flow velocity. Nevertheless, the average velocity always declined if the corrugations get into phase. Ebrahimi *et al.* [14] used the finite volume method to investigate the mixed convection heat transfer of a Cu-water nanofluid in a closed elbow-shaped cavity. They discovered that a higher solid volume fraction improves heat transfer rate.

The double-diffusive combined convection for open cavity has wide range of engineering application such as electronic components cooling, heat exchangers, solar collectors, chemical processing, buildings technology and pollution and thermal control. Many researchers[15-17] have done remarkable investigation on double-diffusive mixed convection and got remarkable motivations. Rashidi *et al.* [17] considered double diffusive mixed convection along with a vertically moving flat plate with a thermal convective boundary condition and hydrodynamic slip.

The base fluid in all the numerical analyses was Newtonian, but due to vast use in industry, many researchers focused on non-Newtonian nanofluids [18-20]. Furthermore, they discovered that when nanoparticles were put to Newtonian fluid, it sometimes exhibited non-Newtonian characteristics. Reza *et al.* [21] used the lattice Boltzmann method to investigate the relationship between thermal radiation and Al_2O_3-water nanofluid in a shallow cavity. They discovered that as Ra increases, the mean heat transfer rate of total natural convection and radiation increases. Barnoon *et al.* [22] numerically studied the entropy generation on nanofluids in horizontal pipes with magnetic effect. They discovered that nanoparticle diameter raises the temperature within the domain, while Hartmann number raises entropy generation. Kole *et al*. [20] reported that added gear oil with copper oxide nanoparticles changed their Newtonian properties to non-Newtonian. A large amount of solid volume fractions of CuO nanoparticles contributed to extensive viscosity rise has also been found. Goodarzi *et al.* [23] investigated the mixed convection of Cu-water nanofluid in a shallow shaped cavity using a 2-phase mixture model and noticed that increasing the solid volume fraction increases the convective heat transfer rate for certain values of Grashof (Gr) and Richardson (Ri). Wei *et al.* [24] simulated a CuO-water nanofluid in a tube. They talked about the follow and heat transfer characteristics of twisted tape, as well as the effect of nanofluid. They noticed that the peak performance occurred because of the twisted tap at 2.18. Mostofazadeh *et al*. [25] investigated radiation of heat transfer characteristics and laminar flow of CuO-water nanofluid in a vertical channel. They found that at constant heat flux and temperature higher solid volume fraction causes the lower velocity contour.

On the other hand, the slip velocity among the nanoparticles and base fluid, is not zero [26]. For this reason, sometimes 2-phase mixture models are used. Buongiorno mathematical model is used to consider the slip mechanisms for Brownian diffusion and thermophoresis between solid and liquid phases[27-29]. Sheikholeslami *et al.* [27] investigated heat transfer and flow for unsteady nanofluid in the magnetic field presence considering the Buongiorno model. They discovered- as the Hartmann number is increased, the corresponding heat transfer rate increases. Later Sheikholeslami and Rokni [28] investigated nanofluid flow on a stretching plate with magnetic effect using the Buongiorno model. They have shown that Heat transfer rate increase with the rise of Hartman number but decreases with increased porosity and melting parameters. In addition to this, Kefayati [29] analyzed non-Newtonian nanofluid mixed convection for key parameters using Buongiorno's mathematical model. He found that heat and mass transfer are notably affected by Brownian motion and thermophoresis parameters.

Based on the foregoing analysis of the literature, it can be concluded that less attention has been paid to studying non-Newtonian nanofluids with a corrugated bottom wall within the enclosure. However, non-

Newtonian nanofluids are important for a variety of engineering applications. The originality of this research is the numerical simulation of non-Newtonian nanofluids of unsteady double diffusive mixed convection flow utilizing Buongiorno's mathematical model with a corrugated bottom wall. To the authors' knowledge, no work has been conducted using Buongiorno's mathematical model on non-Newtonian nanofluid in an enclosure with corrugated bottom wall of unsteady double diffusive mixed convection flow.

Materials and methods

Physical model

The geometry considered for the current problem shown in **Figure 1**. It is composed of a 2-dimensional enclosure with H height. The bottom wall temperature and concentration are considered at high temperature T_h and concentration C_h. In contrast, the upper wall kept at low-temperature T_c and low concentration C_c. The vertical walls happen to be adiabatic. The enclosure is packed with nanofluid that demonstrates shear thinning behavior.

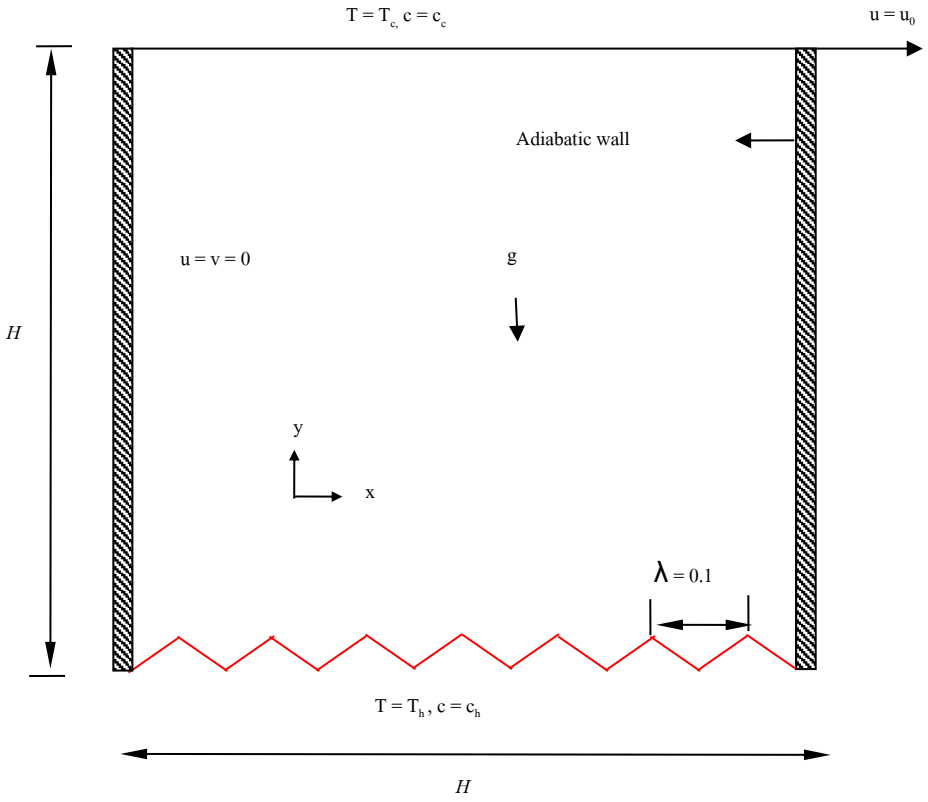

Figure 1 Schematic of the problem with domain and boundary.

Additionally, Brownian motion and thermophoresis parameters were considered. No heating systems, chemical reactions, and heat radiation are considered. The flow is laminar, instable, and incompressible. For both temperature and concentration, the density variance addressed by the standard Boussinesq model.

Mathematical formulation

The 2-dimensional equations governing the problem for the conservation of mass, momentum, and energy are defined in the following dimensional form and taken from [30].

Continuity Equation:

$$\frac{\partial u}{\partial x}+\frac{\partial v}{\partial y}=0 \tag{1}$$

Momentum equation in x-direction:

$$\rho_f\left(\frac{\partial u}{\partial t'}+u\frac{\partial u}{\partial x}+v\frac{\partial u}{\partial y}\right)=-\frac{\partial p}{\partial x}+\left(\frac{\partial \tau'_{xx}}{\partial x}+\frac{\partial \tau'_{xy}}{\partial y}\right) \tag{2}$$

Momentum equation in y-direction:

$$\left.\begin{aligned}\rho_f\left(\frac{\partial v}{\partial t'}+u\frac{\partial v}{\partial x}+v\frac{\partial v}{\partial y}\right)=&-\frac{\partial p}{\partial y}+\left(\frac{\partial \tau'_{yy}}{\partial y}+\frac{\partial \tau'_{xy}}{\partial x}\right)\\&+g\left(\rho_s-\rho_f\right)\left(c-c_c\right)c\\&-g\beta\left(1-c_c\right)\rho_f\left(T-T_C\right)\end{aligned}\right\} \tag{3}$$

Energy Equations:

$$\left.\begin{aligned}\left(\frac{\partial T}{\partial t'}+u\frac{\partial T}{\partial x}+v\frac{\partial T}{\partial y}\right)=&\alpha\left(\frac{\partial^2 T}{\partial x^2}+\frac{\partial^2 T}{\partial y^2}\right)+\delta D_B\left(\frac{\partial c}{\partial x}.\frac{\partial T}{\partial x}+\frac{\partial c}{\partial y}.\frac{\partial T}{\partial y}\right)\\&+\frac{\delta D_T}{T_C}\left[\left(\frac{\partial T}{\partial x}\right)^2+\left(\frac{\partial T}{\partial y}\right)^2\right]\end{aligned}\right\} \tag{4}$$

Conservation equation for the nanoparticles:

$$\left(\frac{\partial c}{\partial t'}+u\frac{\partial c}{\partial x}+v\frac{\partial c}{\partial y}\right)=D_B\left(\frac{\partial^2 c}{\partial x^2}+\frac{\partial^2 c}{\partial y^2}\right)+\frac{D_T}{T_C}\left(\frac{\partial^2 T}{\partial x^2}+\frac{\partial^2 T}{\partial y^2}\right) \tag{5}$$

where x and y happen to be the distances alongside the horizontal and vertical axes respectively, while u and v are the components of velocity in the respective directions; Temperature, concentration, pressure, and density of solid and fluid are denoted by T, c, p, ρ_s and ρ_f respectively. Here gravitational acceleration is g, volumetric coefficient of thermal expansion is β.

Boundary conditions

The followings are the boundary conditions for the current problem:

Upper wall: $u = u_o$, $v = 0$, $T = T_c$, $c = c_c$ (6)

Bottom wall: u = v = 0, T =T_h, c = c_h (7)

Left and right wall: $u=v=\frac{\partial T}{\partial x}=\frac{\partial c}{\partial x}=0$ (8)

The surface average Nusselt number and average Sherwood number were calculated by averaging these local values over the entire heated surface.

$$Nu_{av}=-\frac{1}{H}\int_0^H\frac{\partial T}{\partial y}dx \;\; and \; Sh_{av}=-\frac{1}{H}\int_0^H\frac{\partial c}{\partial y}dx \tag{9}$$

Dimensional analysis

The governing equations (1- 5) are turned into the dimensionless forms using the non-dimensional variables as stated below based on [30]:

$$X=\frac{x}{H},\ Y=\frac{y}{H},\ U=\frac{u}{u_o},\ V=\frac{v}{u_o},\ P=\frac{p}{\rho {u_o}^2},\theta=\frac{(T-T_c)}{(T_h-T_c)},C=\frac{(c-c_c)}{(c_h-c_c)},t'=\frac{tu_o}{H} \tag{10}$$

where X and Y are the coordinates ranging alongside horizontal and vertical directions while U and V happen to be the velocity components in these respective directions, dimensionless temperature is θ and the dimensionless pressure is P. After substituting the dimensionless variables into the equations (1) - (5), below mentioned dimensionless equations are found:

Continuity Equation:

$$\frac{\partial U}{\partial X}+\frac{\partial V}{\partial Y}=0 \tag{11}$$

Momentum equation in x-direction:

$$\frac{\partial U}{\partial t}+U\frac{\partial U}{\partial X}+V\frac{\partial U}{\partial Y}=-\frac{\partial P}{\partial X}+\frac{1}{Re}\left(\frac{\partial \tau_{xx}}{\partial X}+\frac{\partial \tau_{xy}}{\partial Y}\right) \tag{12}$$

Momentum equation in y-direction:

$$\frac{\partial V}{\partial t}+U\frac{\partial V}{\partial X}+V\frac{\partial V}{\partial Y}=-\frac{\partial P}{\partial Y}+\frac{1}{Re}\left(\frac{\partial \tau_{yy}}{\partial Y}+\frac{\partial \tau_{xy}}{\partial X}\right)+RiBrC-Ri\theta \tag{13}$$

Energy Equation:

$$\left.\begin{aligned}\frac{\partial \theta}{\partial t}+U\frac{\partial \theta}{\partial X}+V\frac{\partial \theta}{\partial Y}=\frac{1}{\mathrm{Re}\,\mathrm{Pr}}\left(\frac{\partial^2\theta}{\partial X^2}+\frac{\partial^2\theta}{\partial Y^2}\right)+\frac{1}{\mathrm{Re}\,\mathrm{Pr}}N_b\left[\frac{\partial\theta}{\partial X}\frac{\partial C}{\partial X}+\frac{\partial\theta}{\partial Y}\frac{\partial C}{\partial Y}\right]\\+\frac{1}{\mathrm{Re}\,\mathrm{Pr}}N_t\left[\left(\frac{\partial\theta}{\partial X}\right)^2+\left(\frac{\partial\theta}{\partial Y}\right)^2\right]\end{aligned}\right\} \tag{14}$$

Conservation equation in case of the nanoparticles:

$$\frac{\partial C}{\partial t}+U\frac{\partial C}{\partial X}+V\frac{\partial C}{\partial Y}=\frac{1}{\mathrm{Re}\,\mathrm{Pr}\,Le}\left[\left(\frac{\partial^2 C}{\partial X^2}+\frac{\partial^2 C}{\partial Y^2}\right)+\frac{Nt}{Nb}\left(\frac{\partial^2\theta}{\partial X^2}+\frac{\partial^2\theta}{\partial Y^2}\right)\right] \tag{15}$$

The dimensionless parameters in the Eqs. (12) through (15) are the Prandtl number (*Pr)*, Reynolds number (*Re)*, Richardson number (*Ri)*, Brownian motion (*Nb)*, buoyancy ratio number (*Br)* and thermophoresis parameter (*Nt)*. They are defined below:

$$\left.\begin{aligned}Re=\frac{u_oH}{\upsilon},\ Pr=\frac{\upsilon}{\alpha},Ri=\frac{Gr}{\mathrm{Re}^2}=\frac{(1-c_c)g\beta\Delta TH}{{u_0}^2},Le=\frac{\alpha}{D_B},\\Br=\frac{(\rho_s-\rho_f)\Delta c}{\beta\Delta T\,\rho_f(1-c_c)},Nb=\frac{\delta D_B\Delta c}{\alpha}\ and\ Nt=\frac{\delta D_T\Delta T}{\alpha T_C}\end{aligned}\right\} \tag{16}$$

Where $\Delta T=T_h-T_c,\Delta c=c_h-c_c,\alpha=k/\rho C_p\ and\ \delta=(\rho c)_s/(\rho c)_f$ are the temperature difference, concentration difference, the fluid's thermal diffusivity and ratio between the nanoparticle materials' effective heat capacity and fluids' heat capacity respectively.

The non-dimensional apparent viscosity and stress in case of a non-Newtonian power-law fluid are defined as

$$\eta\left(II\left(A_1\right)\right)=\left\{2\left[\left(\frac{\partial U}{\partial X}\right)^2+\left(\frac{\partial V}{\partial Y}\right)^2\right]+\left(\left(\frac{\partial V}{\partial X}\right)+\left(\frac{\partial U}{\partial Y}\right)\right)^2\right\}^{\frac{n-1}{2}} \tag{17}$$

$$\left.\begin{aligned}\tau_{xx}=2\eta\left(II\left(A_1\right)\right)\left(\frac{\partial U}{\partial X}\right) \quad , \quad \tau_{yy}=2\eta\left(II\left(A_1\right)\right)\left(\frac{\partial V}{\partial Y}\right)\\ \tau_{xy}=\eta\left(II\left(A_1\right)\right)\left(\frac{\partial U}{\partial Y}+\frac{\partial V}{\partial X}\right)\end{aligned}\right\} \tag{18}$$

where n shows fluid flow behavior index. Fluid shows Shear thinning or Pseudoplastic behavior if $n < 1$, the fluid exhibits Newtonian characteristics if $n = 1$ and the fluid shows shear thickening or Dilatant behavior if $1 < n$.
We consider the following dimensionless boundary conditions:

Upper wall: $U = 1, V = 0, \theta = 0, C = 0$ (19)

Bottom wall: $U = V = 0, \theta = C = 1$ (20)

Left and right wall: $U = V = 0$ *and* $\frac{\partial \theta}{\partial X}=\frac{\partial C}{\partial X}=0$ (21)

Evaluation of Physical Quantities of the Model and Stream Function:

Non-Newtonian nanofluid velocity function ψ in terms of U and V is defined by the following equations:

$$U=\frac{\partial \psi}{\partial Y}, V=-\frac{\partial \psi}{\partial X} \tag{22}$$

Stream function calculated by the above equations. Negative sign of ψ presented the clockwise direction and positive sign is for anticlockwise direction.

The average Nusselt number and the average Sherwood number along the heated surface are the 2 significant physical parameters in this model. According to Eq. (22), at the heated wall of the enclosure, the average Nusselt number and Sherwood number based on the non-dimensional variables are:

$$Nu_{av}=-\int_0^1\frac{\partial \theta}{\partial Y}dX \quad and \; Sh_{av}=-\int_0^1\frac{\partial C}{\partial Y}dX \tag{23}$$

where N denotes the non-dimensional distances acting normal to the surface in either the X or Y directions.

Numerical Procedure:

The Galerkin weighted residual finite element method is discussed in this part for solving the non-dimensional governing equations as well as boundary conditions numerically for the phenomena under consideration. The solution technic and calculation procedure are mentioned below.

Computational Procedure with finite element formulation:

Taking the Penalty finite element method [30] in account, Eqs. (12) - (15) is solved. A penalty constraint γ eliminates the pressure P. Thus, the incomprehensible phenomena given by Eq. (11) yields,

$$P=-\gamma\left(\frac{\partial U}{\partial X}+\frac{\partial V}{\partial Y}\right) \tag{24}$$

The continuity equation is immediately satisfied for large values of γ. Using Eqs. (18) and (24) the equations of momentum (12) - (13) reduce to;

$$U\frac{\partial U}{\partial X}+V\frac{\partial U}{\partial Y}=\gamma\frac{\partial}{\partial X}\left(\frac{\partial U}{\partial X}+\frac{\partial V}{\partial Y}\right)+\frac{1}{Re}\left(\frac{\partial^2 U}{\partial X^2}+\frac{\partial^2 U}{\partial Y^2}\right) \tag{25}$$

$$U\frac{\partial V}{\partial X}+V\frac{\partial V}{\partial Y}=\gamma\frac{\partial}{\partial Y}\left(\frac{\partial U}{\partial X}+\frac{\partial V}{\partial Y}\right)+\frac{1}{Re}\left(\frac{\partial^2 V}{\partial X^2}+\frac{\partial^2 V}{\partial Y^2}\right)+Ri\,BrC-Ri\,\theta \tag{26}$$

Flow chart of the computational procedure

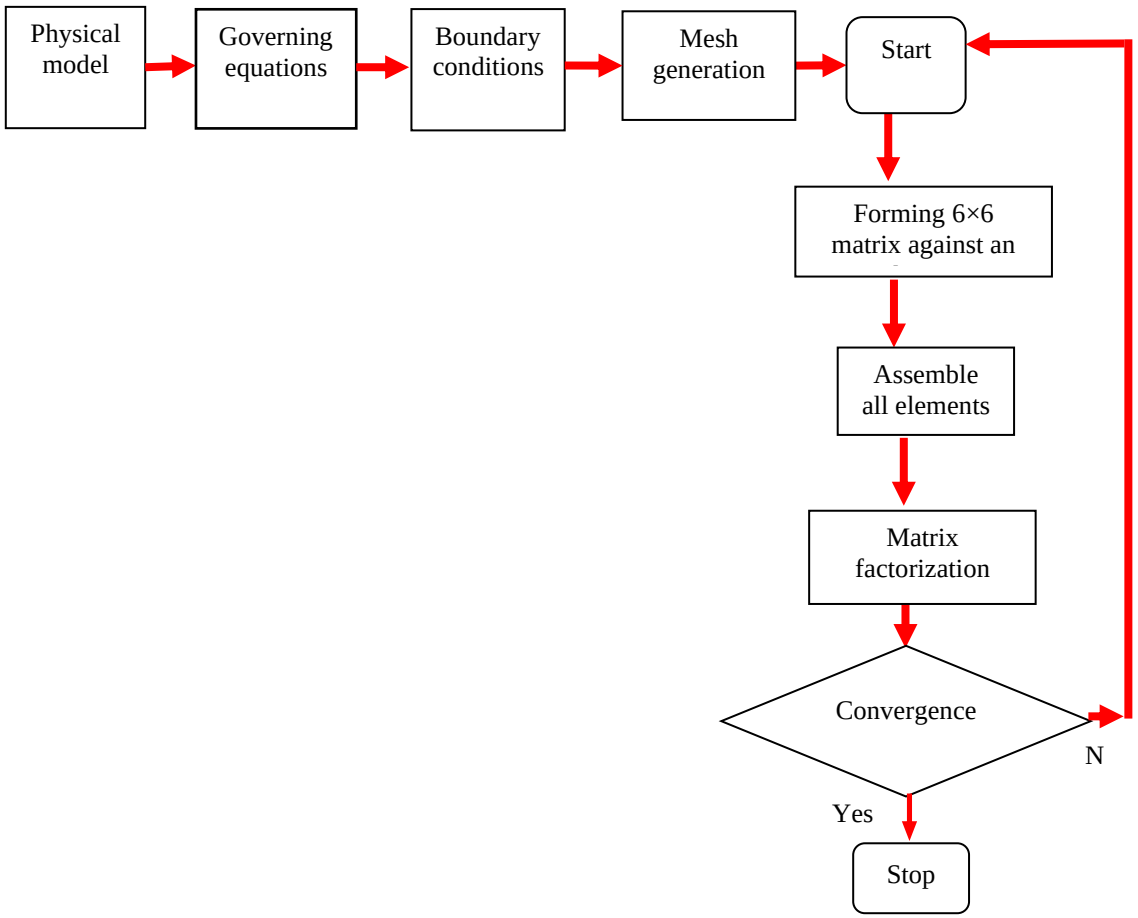

Grid size sensitivity test

To investigate the perfect grid size for the present study, the grid independency test is carried out with *Ri* = 1, *Re* = 100, *Le* = 1, *Nb* = 0.2, *Br* = 0.1, and *Nt* = 0.2. The 7 different non-uniform triangular elements of 3704, 4036, 4675, 5325, 5630, 6245, and 6832 are experienced for the test of grid independency. Due to the sensitivity measure of accuracy and to select the key variables for the grid independency study, the optimum value of the average Nusselt number and Sherwood number of the heated surface and is taken. **Figure 2** shows unique values of Nu_{av} and Sh_{av} at the corresponding considered element. As seen in the figure, the magnitudes of Nu_{av} and Sh_{av} for 5630 elements exhibit an unusually modest fluctuation in comparison to the values found for other higher elements. Based on the accuracy of the obtained numerical values, the simulation is completed with 5630-element grid system.

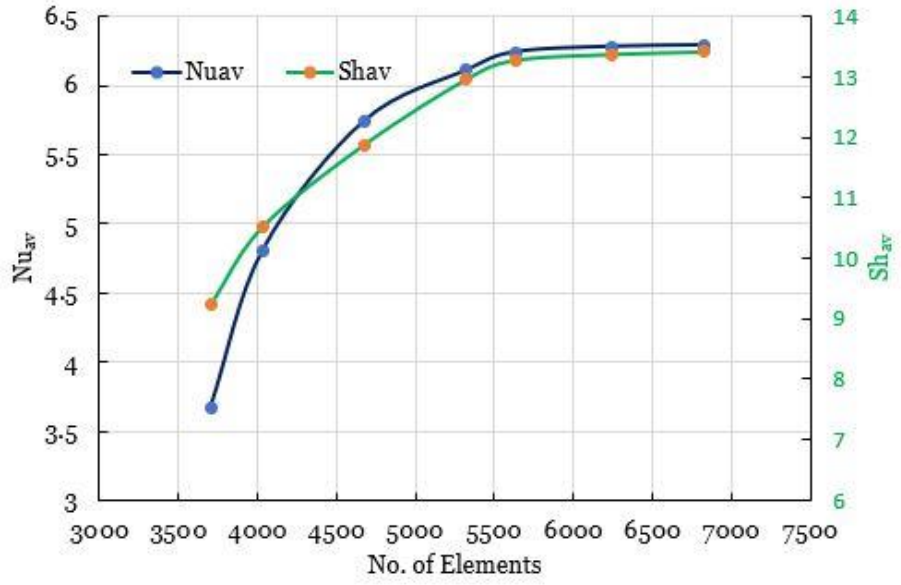

Figure 2 Grid sensitivity check at *Re* = 100, *Ri* = 1, *Le* = 1, *Br* = 0.1, *Nb* = 0.2, *Nt* = 0.2.

Validation of the numerical scheme

Due to a lack of adequate experimental results in the article pertaining to the present system, the obtained numerical results have been confirmed against the likely numerical solution for an open enclosure with a channel. Thus, the current numerical code is validated against the numerical results of Kefayati [29] for mixed convection problem in a lid-driven enclosure. **Table 1** shows the calculated average Nusselt numbers. It is later validated again with Selimefendigil and Chamkha [31]. They used mixed convection of non-Newtonian power law fluid with a lid-driven cavity and a corrugated bottom wall. Sensitivity is measured with v-velocity at a horizontal plane at y = 0.5H from the bottom wall for power-law *n* = 1.4 and *Ri* = 100, as shown in **Figure 3**. The **Table 1** and **Figure 3** demonstrate that the current study's findings are consistent with those previously published findings. As a result, this numerical result of the current investigation has more credibility.

Table 1 Comparison of results of average Nu number for validation at *Br* = 0.1, *Ri* = 0.001, *Le* = 1, *Nb* = 0.1, *Nt* = 0.1, *n* = 0.2.

	Nu_{av}		
Re	**Present**	**Kefayati [17]**	**Error %**
100	2.86	2.09	5.94
400	4.31	4.08	5.33

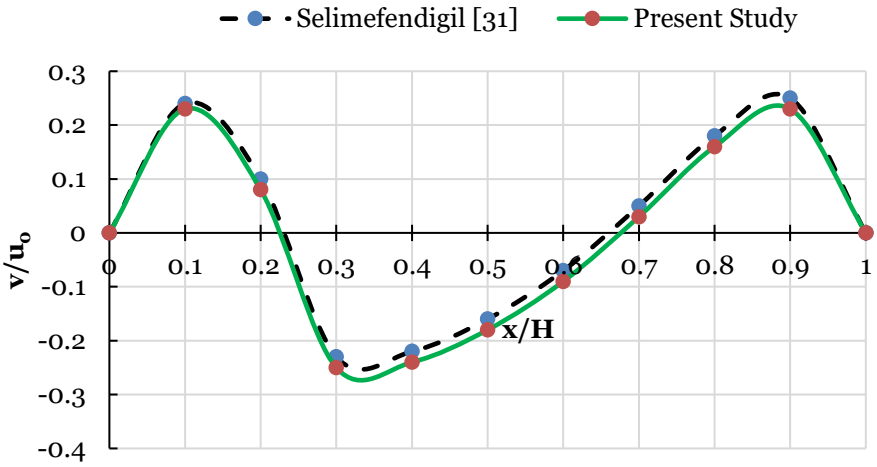

Figure 3 Comparison of v-velocity along the mid of the cavity for *Ri* = 100 and *n* = 1.4, *Ha* = 30, *a* = 0.25H, *b* = 0.1H, and γ = 45°

Results and discussion

Numerical calculations are illustrated to assess the effects of the existence of dimensionless parameters in a square enclosure. The dimensionless parameters to be defined for the system are Richardson number (*Ri)*, Brownian motion parameter (*Nb)*, Lewis number (*Le)* and thermophoresis parameters (*Nt)*. The numerical results would be structured to present different parameters on a specific part of the potential situations through simplification of the configuration. Outcomes of the study represented by the isotherms, streamlines and isoconcentrations patterns in the enclosure. Finally, the average Nusselt number alongside the average Sherwood number in the enclosure will be displayed in graphical form.

Figure 4 represents the flow velocity contour to different values of *Ri* at *t* = 0.1 and 1. It observes that at *t* = 0.1 and *Ri* = 0.1, 2 different vortex sizes are created and cover majority of the enclosure. At the top part of the enclosure, one vortex is formed in a clockwise direction having ψ_{min} = –0.06, and another is the anticlockwise direction with ψ_{max}= 0.01. Also, notice that the higher value of *Ri* = 10 and 15 reinforce the flow velocity. As a result, at *Ri* = 10 vortex magnitude is ψ_{min}= –0.52, ψ_{max} = 0.50 and at *Ri* = 15 is ψ_{min}= –0.65, ψ_{max} = 0.60. Thus, the existence of buoyancy forces is more dominated by increasing *Ri*. Similar pattern of streamline observes for t = 1 at different *Ri.* Moreover, the strength of the flow velocity increase by the higher value of *t*.

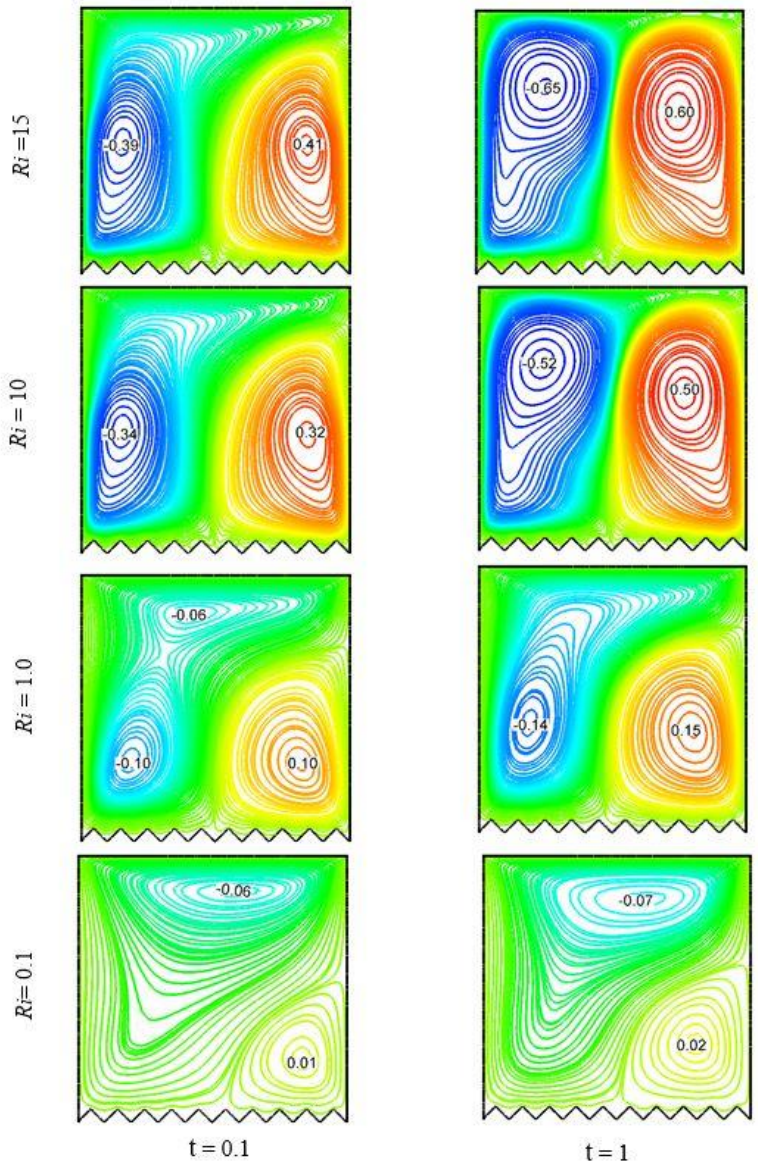

Figure 4 Effect of Richardson number (Ri) on streamlines for the selected values of tat *Br* = 10, *Re* = 100, *Le* = 0.1, *Nb* = 0.1, *Nt* = 0.1.

Figure 5 shows the temperature distribution according to isotherm lines for various values of *Ri* at t = 0.1 and 1. It observes at $t = 0.1$ and 1 for the lower value of *Ri*, near the bottom wall, isotherm lines are grouped together. With an increase in *R*i, the isotherm lines resemble mushroom shape expanding along the vertical walls. At $t = 1$ it looks that for relatively lower *Ri* values, the isotherm lines are a bit closely packed close to the bottom wall. The densities of isotherms are less near the upper part of the enclosure. It indicates that convective heat transfer gradually becomes weak along the upper wall.

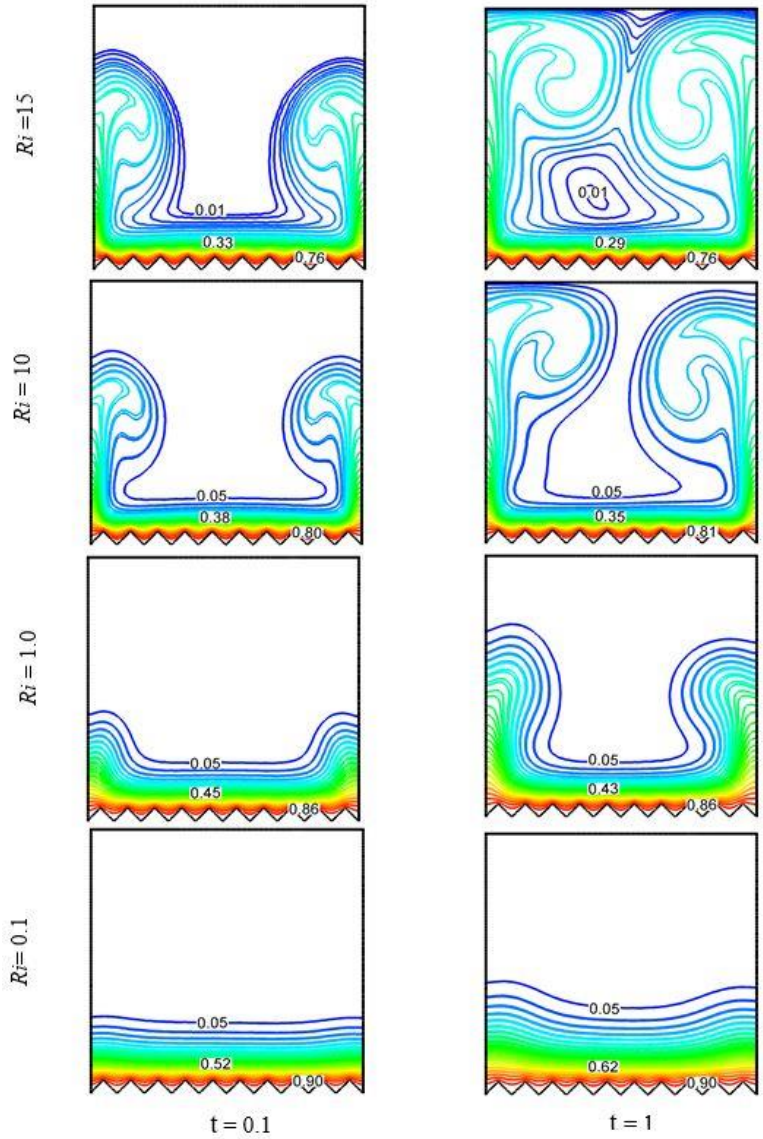

Figure 5 Effect of Richardson number (*Ri*) on isotherms for the selected values of *t* at *Br* = 10, *Re* = 100, *Le* = 0.1, *Nb* = 0.1, Nt = 0.1.

Figure 6 depicts the concentration distribution in terms of iso-concentration lines for different values *Ri* at *t* = 0.1 and 1.0. It is observed from **Figure 5** that the iso-concentration lines are just about parabolic in shape. For *Ri* = 1 and similar behavior for *Ri* = 0.1. As *Ri* increased, the mass lines took more wavy shape. For lower value *Ri* at *t* = 1, the mass lines show a similar pattern.

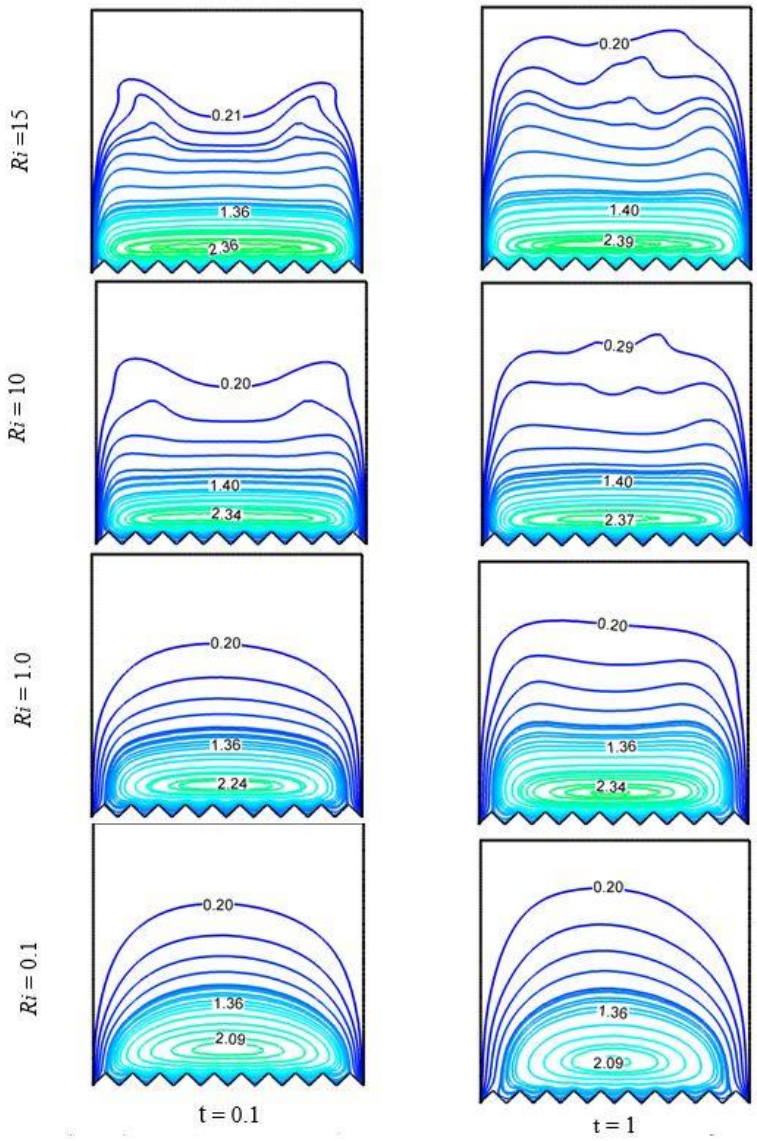

Figure 6 Effect of Richardson number (*Ri*) on iso-concentrations for the selected values of t at *Br* = 10, *Re* = 100, *Le* = 0.1, *Nb* = 0.1, *Nt* = 0.1.

Figure 7 illustrates the outcome of Lewis number on velocity profile by streamlines at $t = 0.1$, and 1. There are 3 different vortices near the walls at 3 sides of the enclosure. Anticlockwise rotation is formed near the top and right walls. On the contrary clockwise rotation is created near left walls. It is because of the force field is acting along the left to right. It also observes that an increase in *Le* flow strength is becoming weaker gradually.

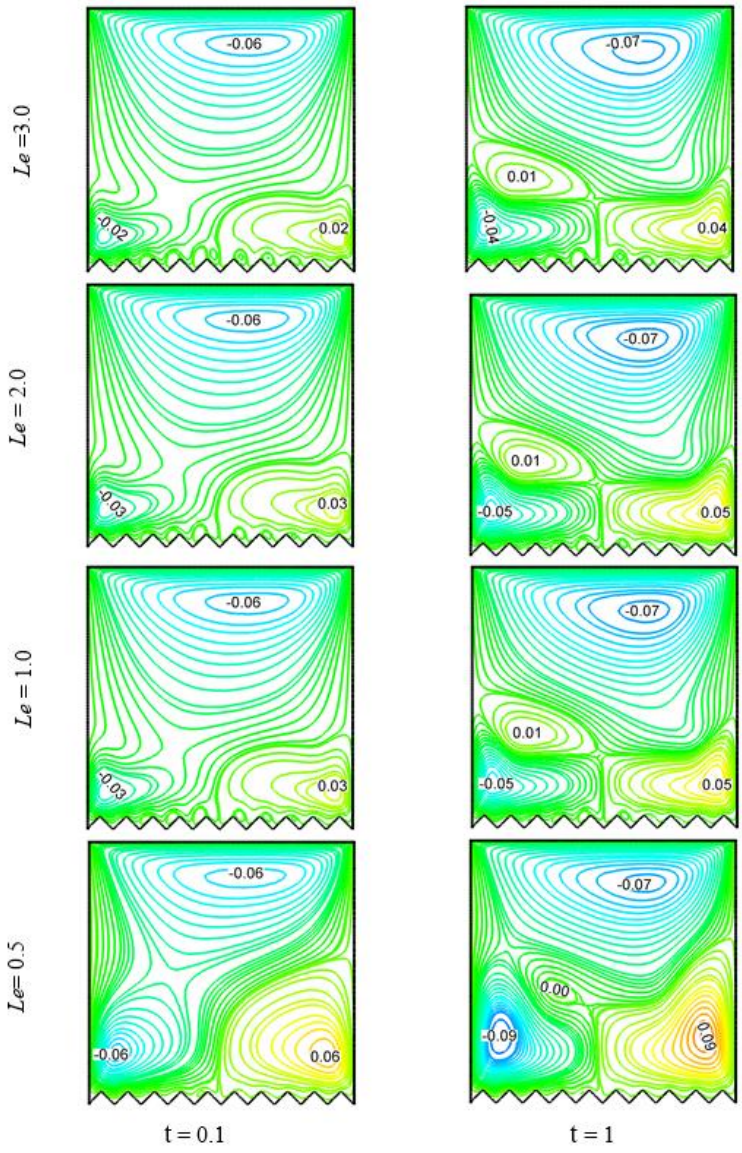

Figure 7 Effect of Lewis number (*Le*) on streamlines for the selected values of tat *Br* = 10, *Ri* = 1, *Re* = 100, *Nb* = 0.1, *Nt* = 0.1.

Figure 8 presents the effects of Lewis number upon temperature distribution. Isothermal lines are clustered closely to the hot wall and less comparable for variation of *Le*. However, minimal variation is noticed for time variation.

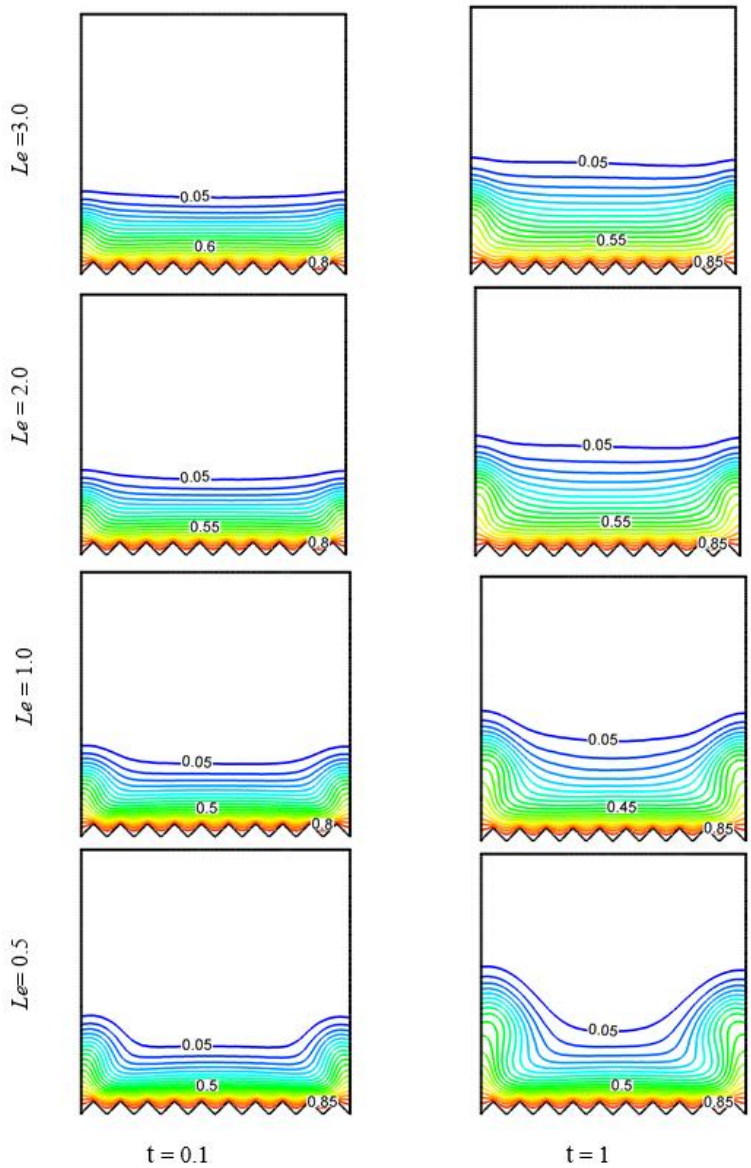

Figure 8 Effect of Lewis number (*Le*) on isotherms for the selected values of tat *Br* = 10, *Ri* = 1, *Re* = 100, *Nb* = 0.1, *Nt* = 0.1.

Figure 9 shows the effect of Lewis number on mass distribution for *t* = 0.1 and 1. From the figure, it looks iso-concentrations contours are dominated by both of an increase of *Le* and t. And due to a decrease in mass diffusivity, it predicts a larger mass transfer.

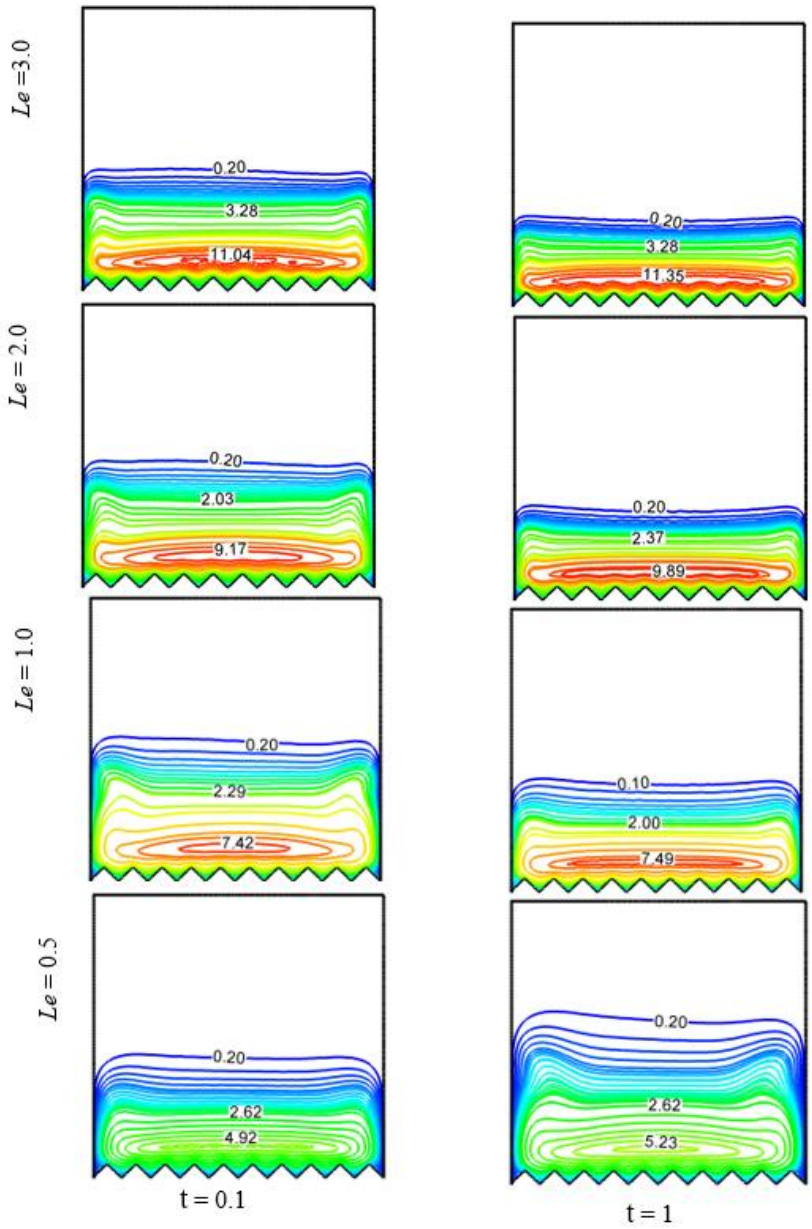

Figure 9 Effect of Lewis number (Le) on iso-concentrations for the selected values of *t* at Br = 10, *Ri* = 1, *Re* = 100, *Nb* = 0.1, *Nt* = 0.1.

The outcome of thermophoresis parameters (*Nt*) on streamlines, isotherms, and iso-concentrations is presented in **Figures 10 - 12**. It is clear from **Figure 10** that flow strength becomes more reliable for an increase of *Nt* and time progresses.

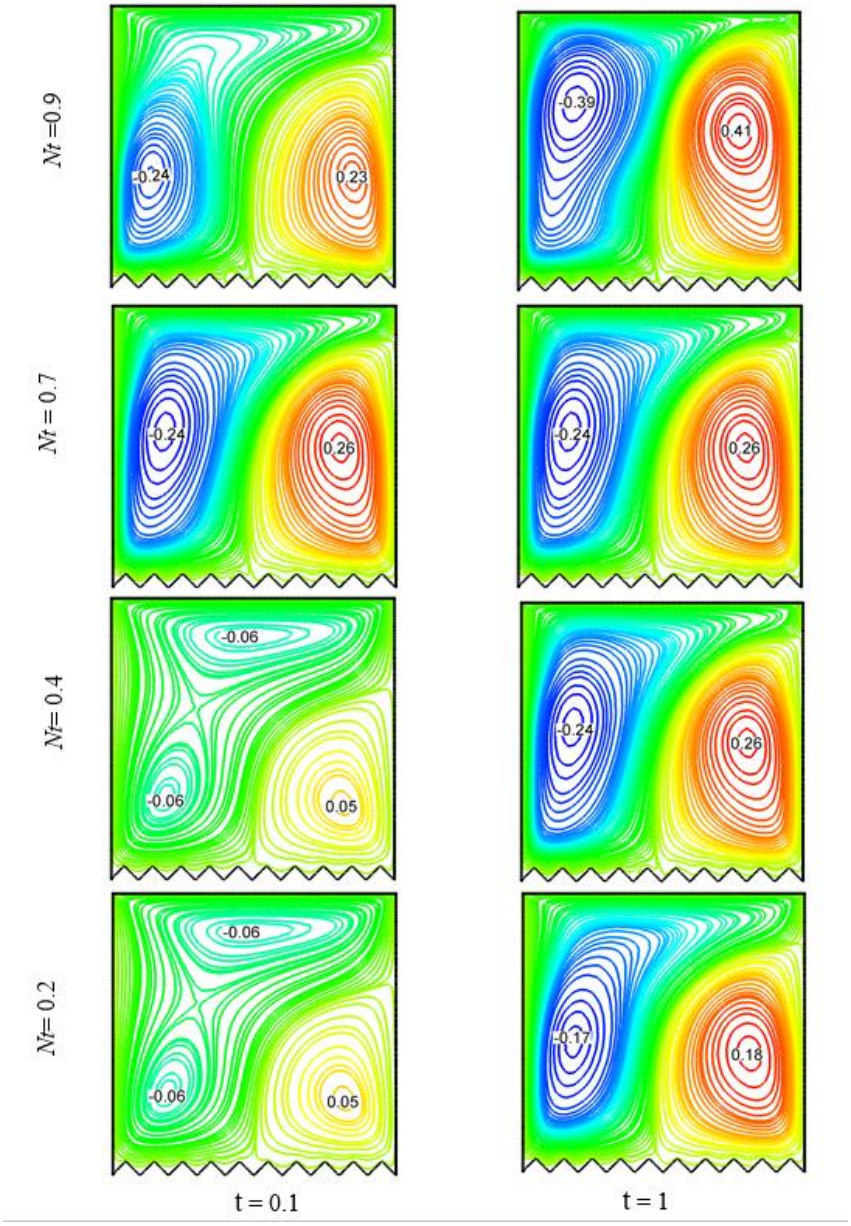

Figure 10 Effect of thermophoresis parameter (*Nt*) on steamlines for the selected values of tat *Br* = 10, *Ri* = 1, *Re* = 100, *Le* = 0.1, *Nb* = 0.1

The outputs of the thermophoresis parameter (*Nt*) on temperature distribution present in **Figure 11**. Due to a decrease in thermal diffusivity, temperature distribution spread well for higher values of *Nt* and time.

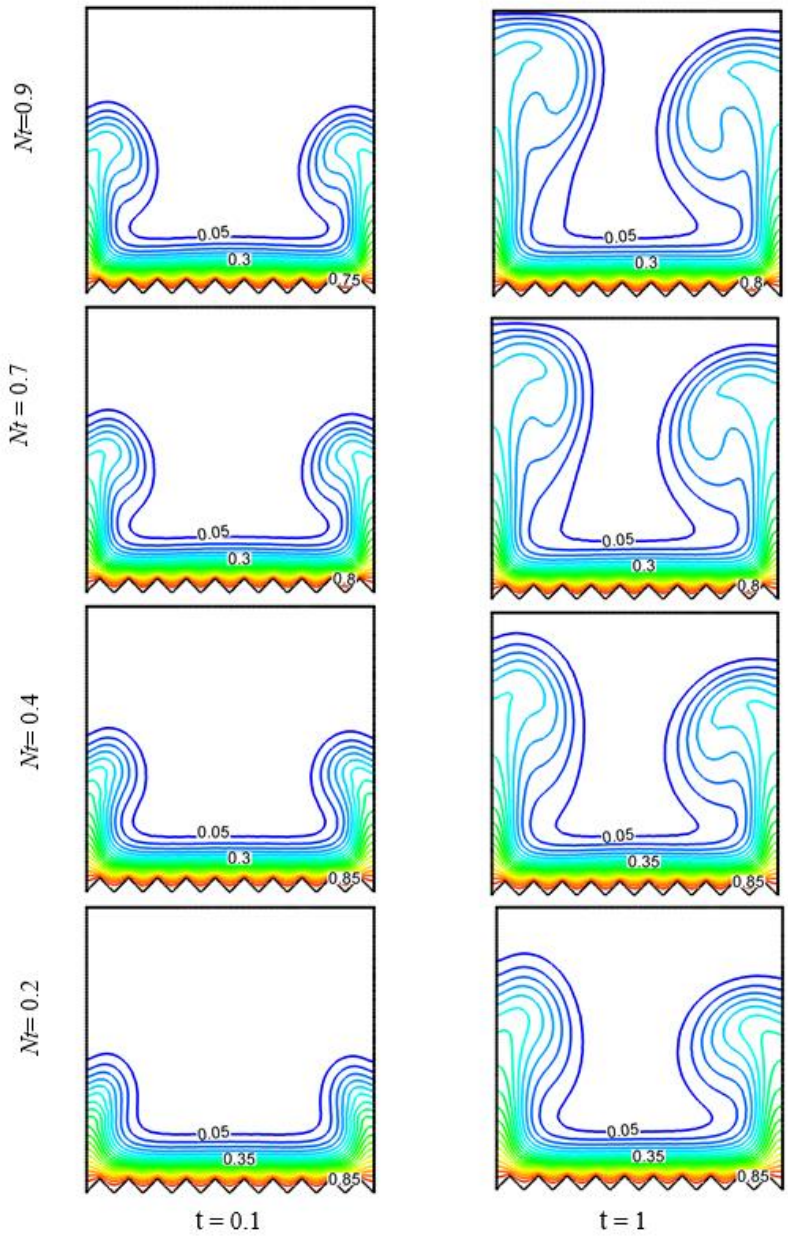

Figure 3 Effect of thermophoresis parameter (*Nt*) on isotherms for the selected values of *t* at *Br* = 10, *Ri* = 1, *Re* = 100, *Le* = 0.1, *Nb* = 0.1.

The results of the thermophoresis parameter upon the isoconcentration profiles within the boundary layer are shown in **Figure 12**. An increase of *Nt* makes comparatively better concentrations. Also, time variation is well dominated upon the concentration.

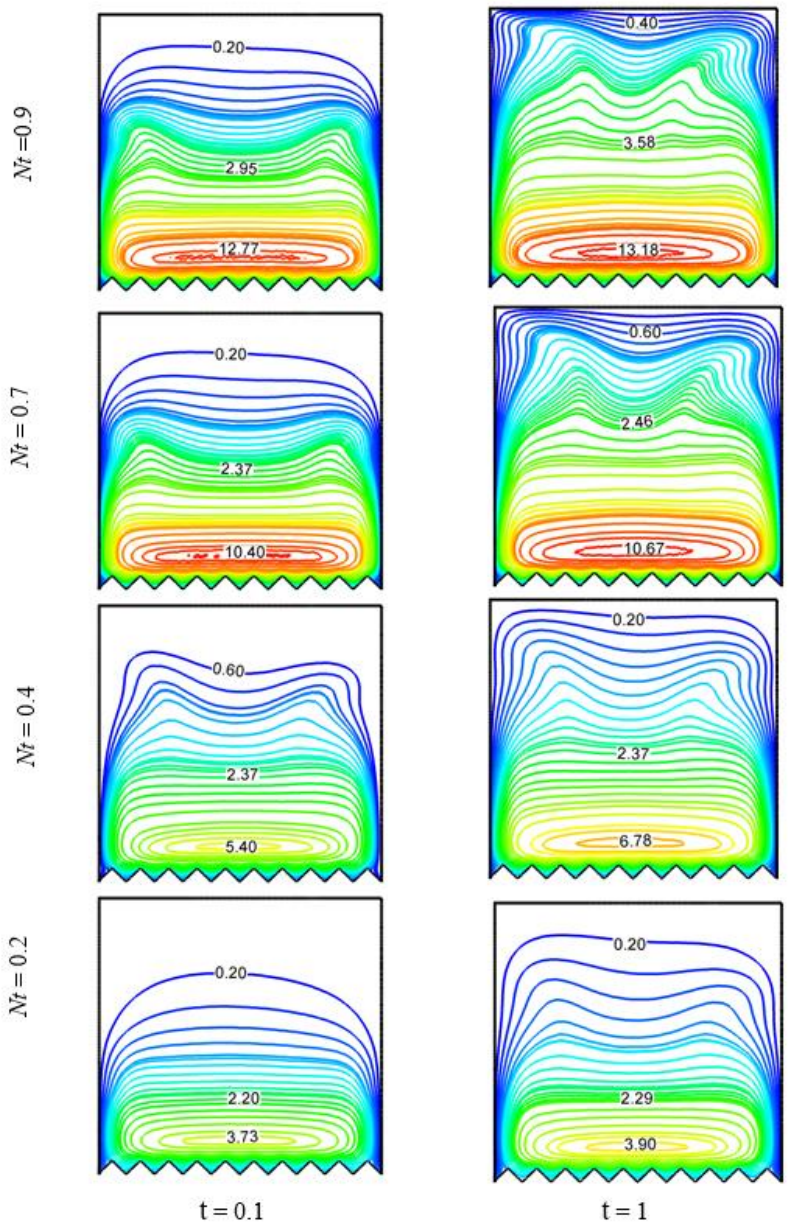

Figure 4 Effect of thermophoresis parameter (*Nt*) on isoconcentrations for the selected values of *t* at *Br* = 10, *Ri* = 1, *Re* = 100, *Le* = 0.1, *Nb* = 0.1.

Figures 13 - 15 illustrate the effects of Brownian motion parameter (*Nb*) for different values. It is evident that there are no significant change as different values of *Nb* on streamlines, isotherms patterns. However, *Nb* shows different valuable change on the isoconcentration profiles at heated corrugated wall.

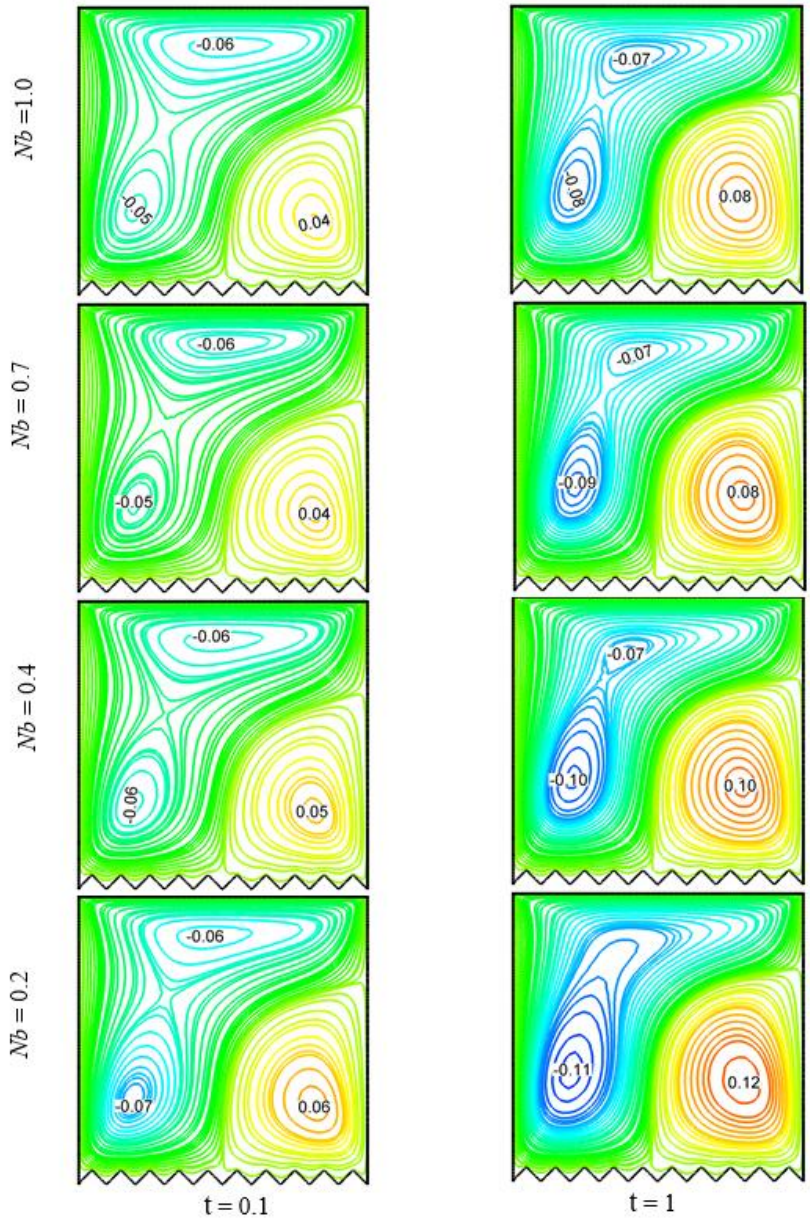

Figure 5 Effect of Brownian motion parameter (*Nb*) on steamlines for the selected values of *t* at *Br* = 10, *Ri* = 1, *Re* = 100, *Le* = 0.1, *Nt* = 0.1.

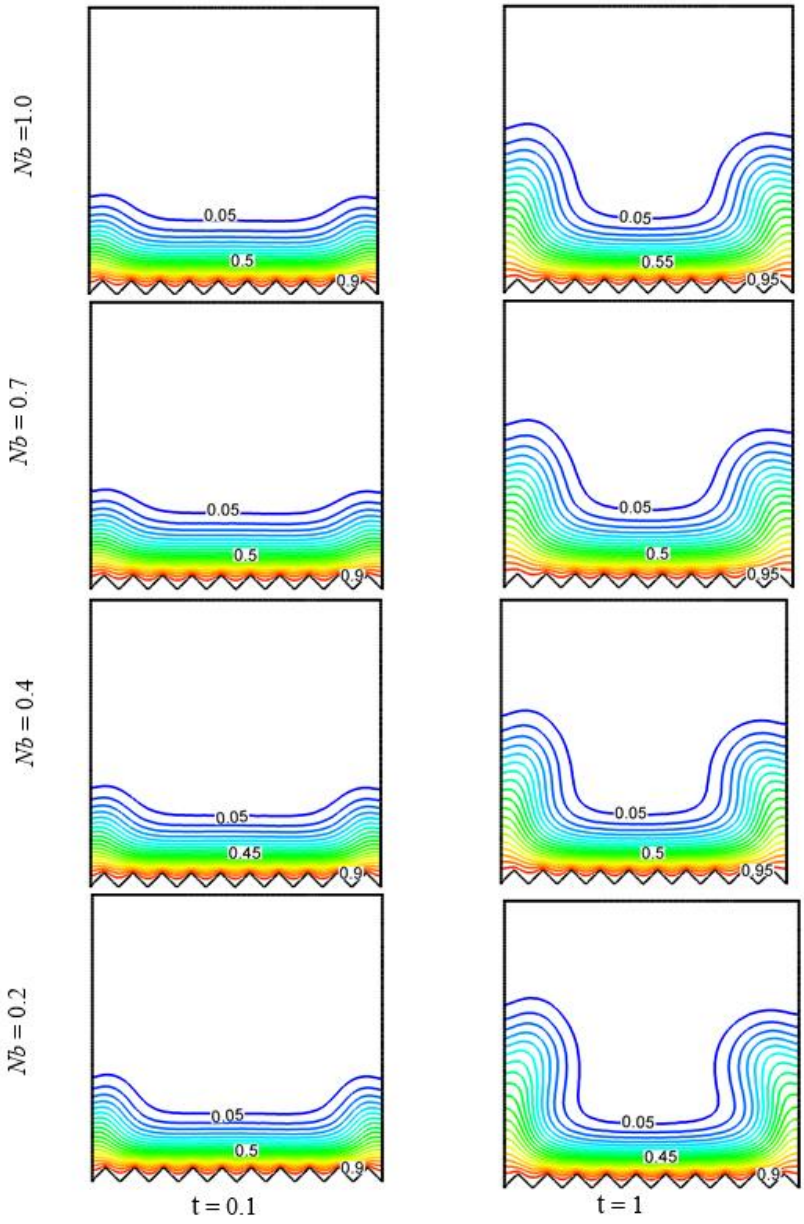

Figure 6 Effect of Brownian motion parameter (*Nb*) on isotherms for the selected values of *t* at Br = 10, *Ri* = 1, *Re* = 100, Le = 0.1, *Nt* = 0.1.

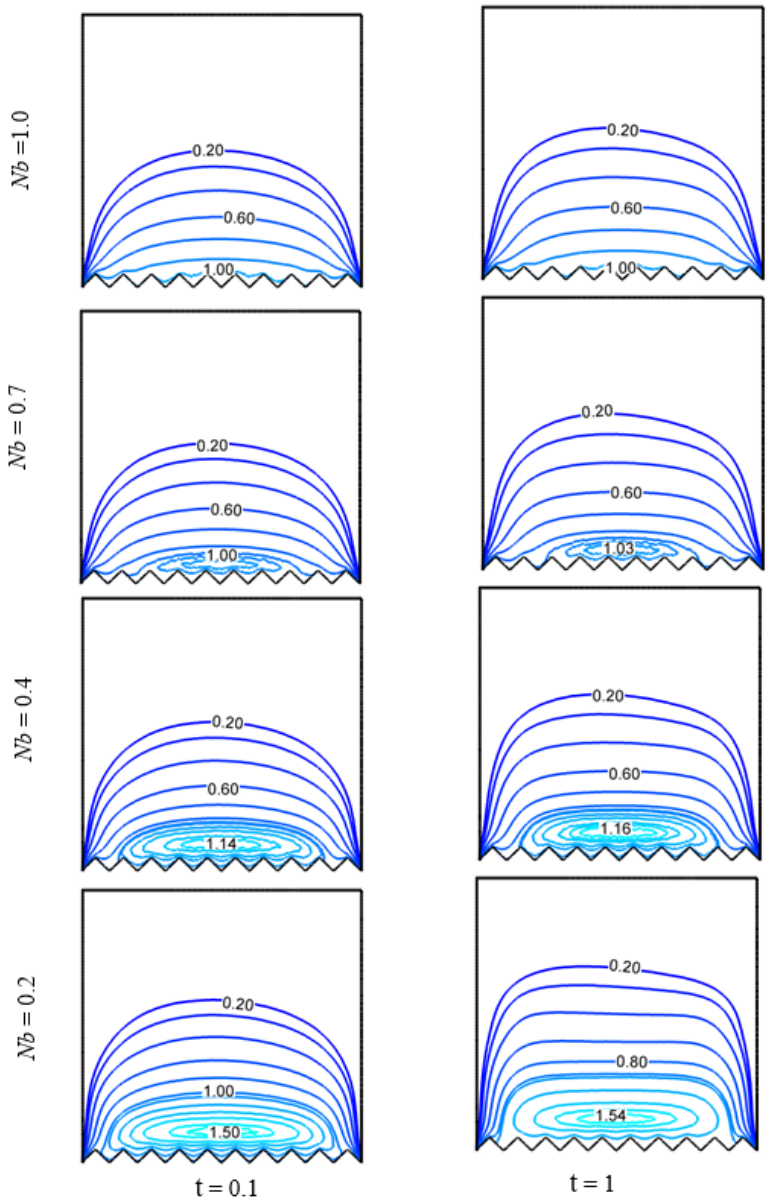

Figure 7 Effect of Brownian motion parameter (*Nb*) on iso-concentrations for the selected values of *t* at *Br* = 10, *Ri* = 1, *Re* = 100, *Le* = 0.1, *Nt* = 0.1.

Figures 16(a) and **16(b)** present line graphs of heat and mass transfer rate for *Ri* as a function of *t*. It observes an increase of *Ri*, both heat and mass transfer rate rise on account of the domination of forced convection. Furthermore, Nu_{av} and Sh_{av} both are exponentially related negatively to time.

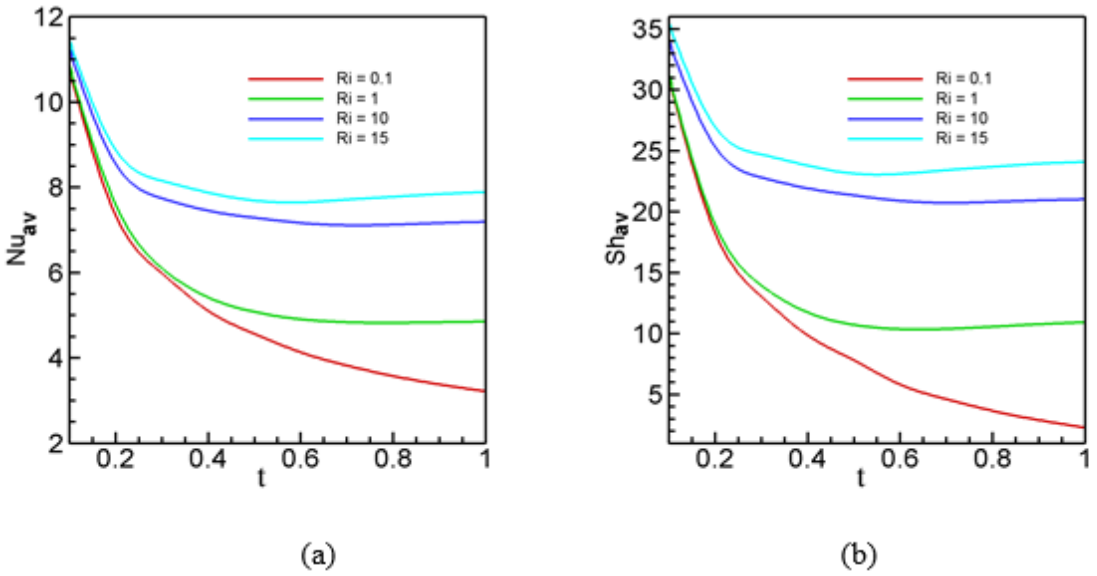

Figure 8 (a) Average Nusselt number and (b) Average Sherwood number at the heated surface verses time for different values of Ri.

The average Nusselt number and Sherwood number at the heat source for a Lewis number are depicted in **Figures 17(a)** and **17(b)** as a function of time. With an increasing value of Le, the average Nusselt number at the heated surface steadily rises. Conversely, With the passage of time, the average Nusselt number values fall exponentially [**Figure 17(a)**]. The same picture observes for the average Sherwood number at the heated wall and is presented in **Figure 17(b)**.

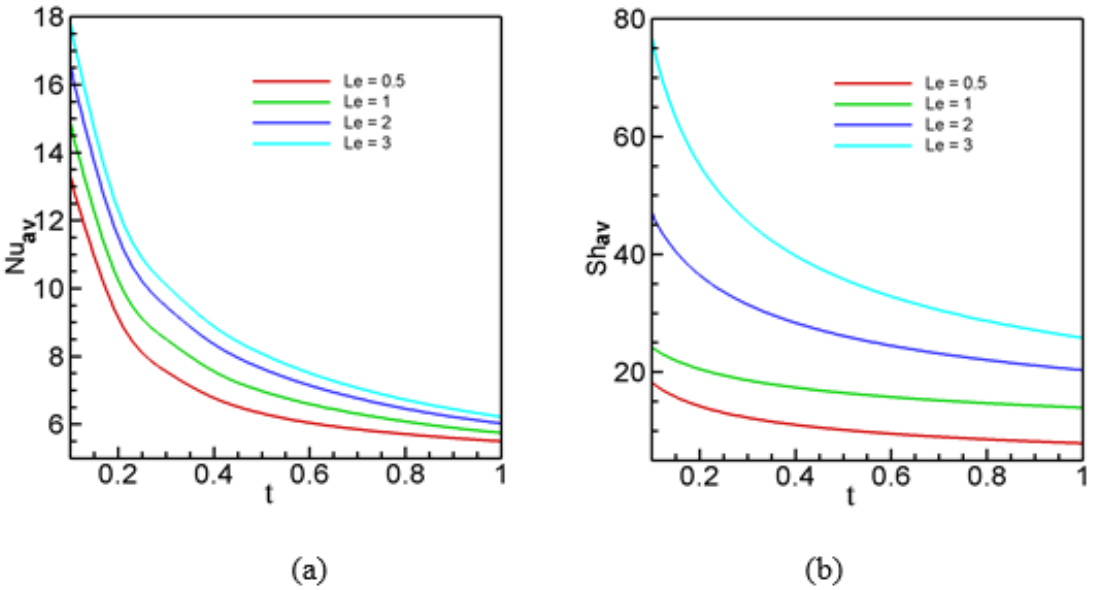

Figure 9 (a) Average Nusselt number and (b) Average Sherwood number at the heated surface verses time for different values of Le.

The average Nusselt number and average Sherwood number at the heated surface for Thermoporesis parameter as a function of time is shown in **Figures 18(a)** and **18(b)**. The average Nusselt number at the heated surface tends to increase with increasing Nt value. However, the average Nusselt number values

exponentially decrease with an increase of time, as seen in **Figure 18(a)**. A similar phenomenon observed for Sherwood number and plotted in **Figure 18(b)**.

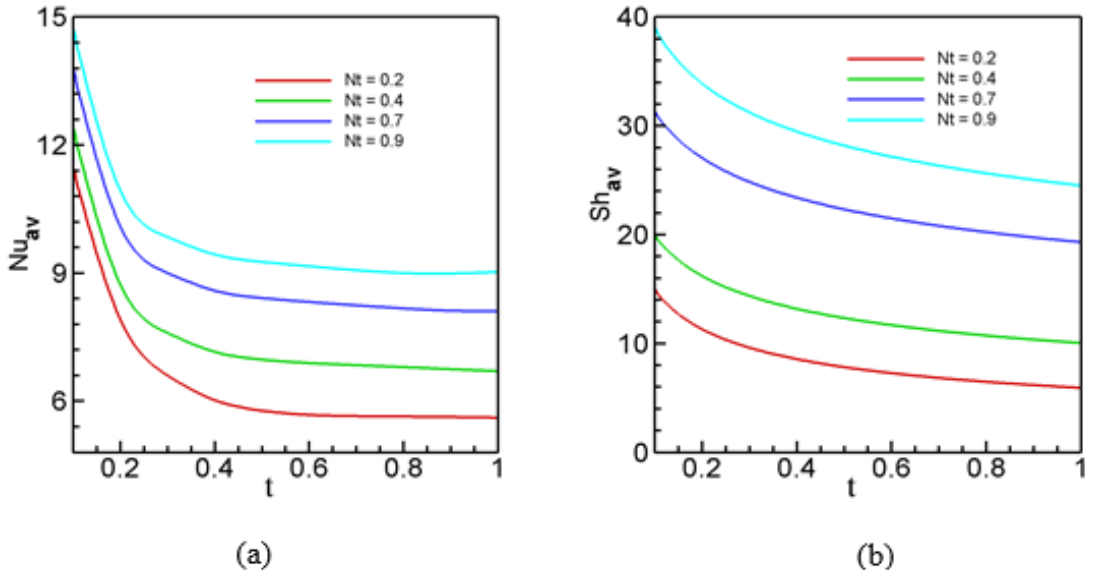

Figure 10 (a) Average Nusselt number and (b) Average Sherwood number at the heated surface verses time for different values of *Nt*.

However, opposite significant change is seen for the values of *Nb* average heat and mass transfer rate in **Figures 19(a)** and **19(b)**.

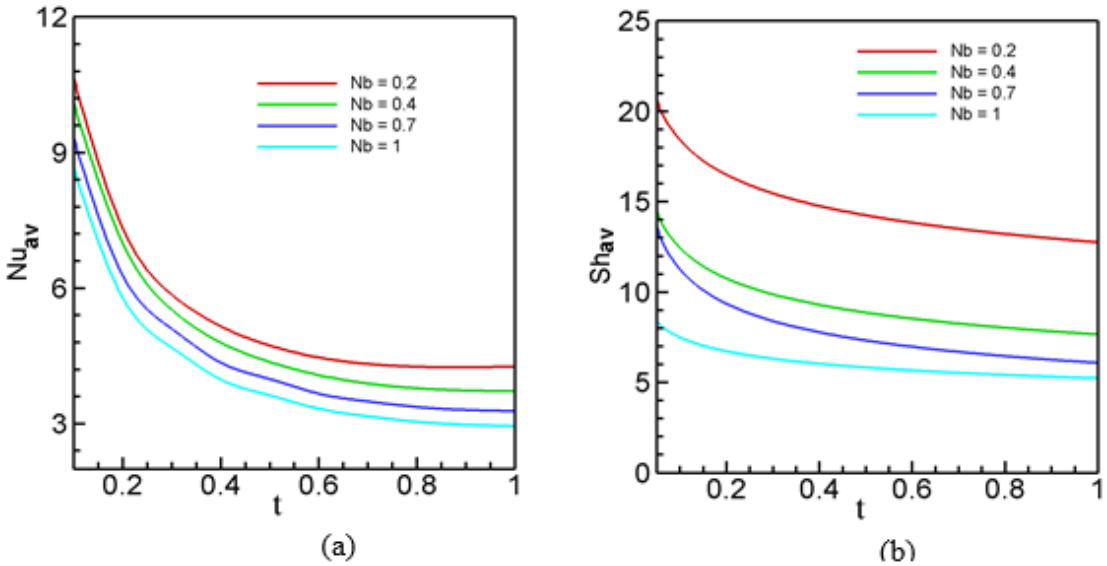

Figure 19 (a) Average Nusselt number and (b) Average Sherwood number at the heated surface verses time for different values of *Nb*.

Conclusions

The computational evaluation has been performed within a square enclosure with corrugated bottom wall with the use of Buongiorno's mathematical model. Followings are the enhancing performance of this model that can be used in process engineering design approached to predict the heat and mass transfer rate from the heated surface. The notable findings of this study are given bellow:

Ri has a significant effect on the thermal and flow fields inside the enclosure, as well as on the rate of heat transfer.

The Lewis number (*Le*) has a minor effect on flow and thermal fields. Increasing *Le* values have no discernible influence on streamlines. However, when *Le* increases, the isotherm lines appear practically identically. Nonetheless, mass transfer is heavily influenced by *Le*. The strength of the concentration outlines increases as the value of *Le* rises. Finally, as *Le* increases, the heat and mass transfer rates increase, implying that as thermal diffusivity increases, mass diffusivity naturally declines for increasing values of Lewis number.

The influence of the thermophoresis parameter (*Nt*) demonstrates that the effect of *Nt* on velocity is less important, but it is considerably more significant on isotherm lines and iso-concentrations. Although the values of average *Nu* and average *Sh* increase with increasing *Nt* values, these numbers drop over time.

The Brownian motion parameter (*Nb*) has a significant effect on isotherm lines and iso-concentration profiles. The addition of *Nb* decreases the temperature and volume concentration of nanoparticles, implying that the average heat and mass transfer rates decrease progressively as *Nb* concentration increases.

Acknowledgements

The authors like to express their gratitude to the Bangladesh University of Engineering and Technology (BUET) for providing financial support under the Basic Research Grant No. 1111202109017.

References

[1] CSK Raju, N Sandeep and A Malvandi. Free convective heat and mass transfer of MHD non-Newtonian nanofluids over a cone in the presence of non-uniform heat source/sink. *J. Mol. Liq.* 2016; **221**, 108-15.

[2] AK Azad, MM Shuvo, RH Kabir, KM Rabbi, MF Karim and MM Rahman. Heat transfer augmentation in a diamond shaped enclosure utilizing CNT-water Nanofluid. *Int. Commun. Heat Mass Transf.* 2020; **116**, 104647.

[3] AR Rahmati, OA Akbari, A Marzban, D Toghraie, R Karimi and F Pourfattah. Simultaneous investigations the effects of non-Newtonian nanofluid flow in different volume fractions of solid nanoparticles with slip and no-slip boundary conditions. *Therm. Sci. Eng. Prog.* 2018; **5**, 263-77.

[4] S Nazari, R Ellahi, MM Sarafraz, MR Safaei, A Asgari and OA Akbari. Numerical study on mixed convection of a non-Newtonian nanofluid with porous media in a two lid-driven square cavity. *J. Therm. Anal. Calorim.* 2020; **140**, 1121-45.

[5] SS Pawar and VK Sunnapwar. Experimental studies on heat transfer to Newtonian and non-Newtonian fluids in helical coils with laminar and turbulent flow. *Exp. Therm. Fluid Sci.* 2013; **44**, 792-804.

[6] Z Li, P Barnoon, D Toghraie, R Balali Dehkordi and M Afrand. Mixed convection of non-Newtonian nanofluid in an H-shaped cavity with cooler and heater cylinders filled by a porous material: Two phase approach. *Adv. Powder Technol.* 2019; **30**, 2666-85.

[7] M Yoshino, Y Hotta, T Hirozane and M Endo. A numerical method for incompressible non-Newtonian fluid flows based on the lattice Boltzmann method. *J. Nonnewton. Fluid Mech.* 2007; **147**, 69-78.

[8] MA Ahmed, MZ Yusoff and NH Shuaib. Effects of geometrical parameters on the flow and heat transfer characteristics in trapezoidal-corrugated channel using nanofluid. *Int. Commun. Heat Mass Transf.* 2013; **42**, 69-74.

[9] M Goodarzi, AD Orazio, A Keshavarzi, S Mousavi and A Karimipour. Develop the nano scale method of lattice Boltzmann to predict the fluid flow and heat transfer of air in the inclined lid driven cavity with a large heat source inside, Two case studies: Pure natural convection & mixed convection. *Phys. A Stat. Mech. its Appl.* 2018; **509**, 210-33.

[10] MM Rahman, R Saidur, S Mekhilef, MB Uddin and A Ahsan. Double-diffusive buoyancy induced flow in a triangular cavity with corrugated bottom wall: Effects of geometrical parameters. *Int. Commun. Heat Mass Transf.* 2013; **45**, 64-74.

[11] SA Rozati, F Montazerifar, OA Akbari, S Hoseinzadeh, V Nikkhah, A Marzban, H Abdolvand and M Goodarzi. Natural convection heat transfer of water/Ag nanofluid inside an elliptical enclosure with different attack angles. *Math. Methods Appl. Sci.* 2020. https://doi.org/10.1002/mma.7036
[12] A Aghaei, GA Sheikhzadeh, M Goodarzi, H Hasani, H Damirchi and M Afrand. Effect of horizontal and vertical elliptic baffles inside an enclosure on the mixed convection of a MWCNTs-water nanofluid and its entropy generation. *Eur. Phys. J. Plus* 2018; **133**, 486.
[13] M Buren, Y Jian and L Chang. Electromagnetohydrodynamic flow through a microparallel channel with corrugated walls. *J. Phys. D. Appl. Phys.* 2014; **47**, 425501.
[14] D Ebrahimi, S Yousefzadeh, OA Akbari, F Montazerifar, SA Rozati, S Nakhjavani and MR Safaei. Mixed convection heat transfer of a nanofluid in a closed elbow-shaped cavity (CESC). *J. Therm. Anal. Calorim.* 2021; **144**, 2295-316.
[15] AK Azad, MJH Munshi and MM Rahman. Double diffusive mixed convection in a channel with a circular heater. *Procedia Eng.* 2013; **56**, 157-62.
[16] MB Uddin, MM Rahman and MAH Khan. Hydromagnetic double-diffusive unsteady mixed convection in a trapezoidal enclosure due to uniform and nonuniform heating at the bottom side. *Numer. Heat Transf. A: Appl.* 2015; **68**, 205-24.
[17] MM Rashidi, N Kavyani, S Abelman, MJ Uddin and N Freidoonimehr. Double diffusive magnetohydrodynamic (MHD) mixed convective slip flow along a radiating moving vertical flat plate with convective boundary condition. *PLoS One*. 2014; **9**, 109404.
[18] Q Xiong, MV Bozorg, MH Doranehgard, K Hong and G Lorenzini. A CFD investigation of the effect of non-Newtonian behavior of Cu-water nanofluids on their heat transfer and flow friction characteristics. *J. Therm. Anal. Calorim.* 2020; **139**, 2601-21.
[19] L Yang and K Du. A comprehensive review on the natural, forced, and mixed convection of non-Newtonian fluids (nanofluids) inside different cavities. *J. Therm. Anal. Calorim.* 2020; **140**, 2033-54.
[20] M Kole and TK Dey. Effect of aggregation on the viscosity of copper oxide-gear oil nanofluids. *Int. J. Therm. Sci.* 2011; **50**, 1741-7.
[21] MR Safaei, A Karimipour, A Abdollahi and TK Nguyen. The investigation of thermal radiation and free convection heat transfer mechanisms of nanofluid inside a shallow cavity by lattice Boltzmann method. *Phys. A: Stat. Mech. Appl.* 2018; **509**, 515-35.
[22] P Barnoon, D Toghraie, F Eslami and B Mehmandoust. Entropy generation analysis of different nanofluid flows in the space between two concentric horizontal pipes in the presence of magnetic field: Single-phase and two-phase approaches. *Comput. Math. Appl.* 2019; **77**, 662-92.
[23] M Goodarzi, MR Safaei, K Vafaic, G Ahmadi, M Dahari, SN Kazi and N Jomhari. Investigation of nanofluid mixed convection in a shallow cavity using a two-phase mixture model. *Int. J. Therm. Sci.* 2014; **75**, 204-20.
[24] W He, D Toghraie, A Lotfipour, F Pourfattah, A Karimipour and M Afrand. Effect of twisted-tape inserts and nanofluid on flow field and heat transfer characteristics in a tube. *Int. Commun. Heat Mass Transf.* 2020; **110**, 104440.
[25] A Mostafazadeh, D Toghraie, R Mashayekhi and OA Akbari. Effect of radiation on laminar natural convection of nanofluid in a vertical channel with single- and two-phase approaches. *J. Therm. Anal. Calorim.* 2019; **138**, 779-4.
[26] J Buongiorno. Convective transport in nanofluids. *J. Heat Transf.* 2006; **128**, 240-50.
[27] M Sheikholeslami, DD Ganji and MM Rashidi. Magnetic field effect on unsteady nanofluid flow and heat transfer using Buongiorno model. *J. Magn. Magn. Mater.* 2016; **416**, 164-73.
[28] M Sheikholeslami and HB Rokni. Effect of melting heat transfer on nanofluid flow in existence of magnetic field considering Buongiorno Model. *Chinese J. Phys.* 2017; **55**, 1115-26.
[29] GHR Kefayati. Mixed convection of non-Newtonian nanofluid in an enclosure using Buongiorno's mathematical model. *Int. J. Heat Mass Transf.* 2017; **108**, 1481-500.
[30] Mawa and H Zannatul. Numerical solution of non-newtonian nanofluid using buongiorno's mathematical model, Available: http://lib.buet.ac.bd:8080/xmlui/handle/123456789/5785, accessed January 2022.
[31] F Selimefendigil and AJ Chamkha. Magnetohydrodynamics mixed convection in a lid-driven cavity having a corrugated bottom wall and filled with a non-newtonian power-law fluid under the influence of an inclined magnetic field. *J. Therm. Sci. Eng. Appl.* 2016; **8**, 021023.